Effect of Valves Stiffness on the Performance of a Twin-Tube Hydraulic Damper

AMINA BEN ABDELWAHED, JAMEL CHAKHARI, CHARFEDDINE MRAD
Laboratory of Applied Mechanics and Engineering,
National Engineering School of Tunis, University of Tunis El Manar,
Tunis 1002,
TUNISIA

Abstract: - In this paper, the dynamic behavior of a twin-tube automotive hydraulic damper is studied. A front axle car damper is subjected to experiments in both phases compression and rebound. Accurate CFD simulations are developed to improve the understanding of the performance of the damper by exploring its hydraulic behaviors in transient response. Dynamic meshing is applied to simulate the fluid flow in terms of velocity and pressure distribution in damper chambers. The deflections of base and piston valve membranes respectively in compression and rebound are determined through an iterative method considering the fluid-structure coupling. Numerical results are in good correlation with those issued from experiments. The presented CFD model is a numerical tool if applied can minimize the number of experiments in the step of design and testing of twin-tube dampers.

Key-Words: - Twin-tube hydraulic damper, Compression and rebound, Force-velocity curves, Valve configurations, Membranes deflection, Testing of prototype, CFD simulation, Transient flow.

Received: April 16, 2024. Revised: October 22, 2024. Accepted: November 9, 2024. Published: December 21, 2024.

1 Introduction

The suspension on a vehicle is the term given to the system composed of springs, dampers, and mechanical links that connect the vehicle chassis to the axles. Because of irregularities of some roads, a running car can be subjected to different displacements which greatly reduce the comfort of passengers. Shock absorbers limit the oscillatory movements, slow the bouncing of the wheels on obstacles, and keep them in contact with the ground. In order to lower the amplitude of vibration, all sorts of shock absorbers are used. The hydraulic damper is the main component of such systems.

Several studies have been carried out on hydraulic dampers ; experimental characterization, [1], [2], [3], [4], [5] and especially modeling [6], [7], [8]. For characterization, car manufacturers use a simple force-velocity curve as a computer model of the damper. An experimental or numerical curve should be found between two standard limit curves for quality control and damper acceptance.

Hydraulic dampers that are used in recent vehicles have characteristics that are generally unsymmetrical and nonlinear. The damper is one of the most difficult components to model because of its highly nonlinear characteristics, [9]. In many papers, researchers studied the twin-tube damper type. A physical and mathematical nonlinear model was created for a twin-tube hydraulic damper. To analyze the theoretical model, methods of numerical integration were incorporated, [10]. The characteristics of the damping force depend mainly on the geometrical and physical properties of the top and bottom valves of the damper. This conclusion is deduced also in research references [11] and [12], where force displacement and force-time plots are considered for damper characteristics analysis.

In paper [13], a numerical model was used to show the advantage of a base valve to make a twin-tube damper more performant than a mono-tube one. In numerous published papers, the effect of design parameters on hydraulic damper behavior is shown. The the effect of number of orifices on the damping force at different velocities for a two-wheeler automobile mono-tube damper is investigated, [14]. It is concluded that as the number of orifices increases the damping force and the damping coefficient decrease. The simulation of failure characteristics of a twin-tube shock absorber is done to show limit curves, [15]. The dynamic stiffness and damping coefficients are computed under multiple conditions. A nonlinear model is established in order to analyze the effects of shim stack and orifice parameters on damper performance, [16]. The model helps in developing controllable valving based on shim stacks in dampers. Results of the CFD orifice flow model of hydraulic oil presented in reference [17], show that orifices are employed to damp pressure pulsation to improve the system control accuracy. In some conditions the flow regime transition from laminar to turbulence can be obtained, which affects the valve membrane's deflection and therefore the damper response.

In this context, this work consists of studying experimentally and by CFD simulation the dynamic behavior of a twin-tube hydraulic damper for front axle of vehicles. Characteristic curves will be plotted for several excitation velocities and for different configurations of valves, in compression and rebound. We interested mainly in transient phase of damping. A dynamic meshing will be used to study the fluid transient flow.

In addition to orifices, the piston and base valves in a twin-tube damper consists of a stack of thin membranes. The best configuration of membranes, numbers, and thickness, will be chosen. The deflection of these membranes under fluid pressure passing through valves orifices will be determined. It consists of showing how the geometry of the dual-tube automotive damper affects its hydraulic behavior and its performance.

In comparison with the corresponding studies of other researchers, cited previously, the novelty in this paper is the iterative method applied for determining the shim stack deflection by coupling with the CFD model of fluid domain. That deflection controls all the hydraulic damper response.

2 Design and Operating Phases of a Twin-Tube Damper

The damper under study is a subassembly of a twin-tube shock absorber for the automotive front axle. It consists mainly of two coaxial tubes or cylinders as shown in Figure 1.

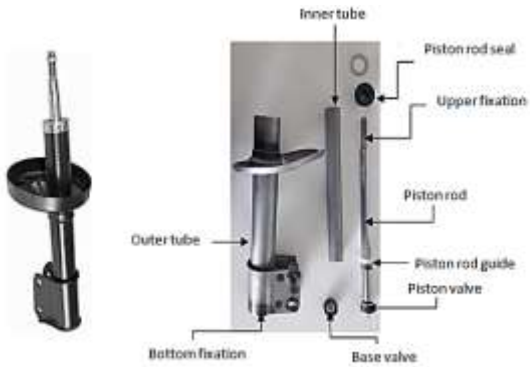

Fig. 1 : Damper components

The chamber in which the piston and rod move is the working chamber. The compensation chamber is located between the inner tube and the body tube. It is filled 2/3 with oil and 1/3 with air or gas. Compared to single-tube construction, twin-tube dampers offer the advantage of being shorter. In twin-tube dampers, base valve and piston valve consist of a system of small spring washers or thin elastic membranes. The piston or base valves have throttle holes for the passage of oil. The rod, guide, and seal are extremely precise components.

The damper consists of three chambers. An external compensation chamber and two internal working chambers. Inside the working cylinder, the piston is attached to the rod, and it separates the two internal chambers. The piston rod is equipped with a guide that limits its movement in the longitudinal direction, Figure 2. The characteristic curves of the damping force are specially determined for each type of vehicle, taking into account the weight of the vehicle, the construction of the axles, and the chassis springs stiffness.

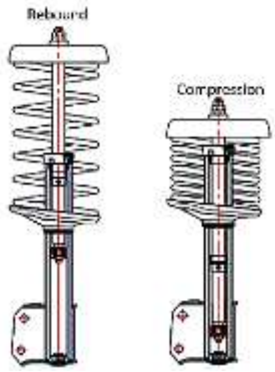

Fig. 2 : Operating phases of shock absorbers

During the rebound phase, the fluid in the expansion chamber is forced to flow to the compression one. During the compression phase, the fluid in the compression chamber is forced to flow to the expansion and compensation chambers, Figure 3.

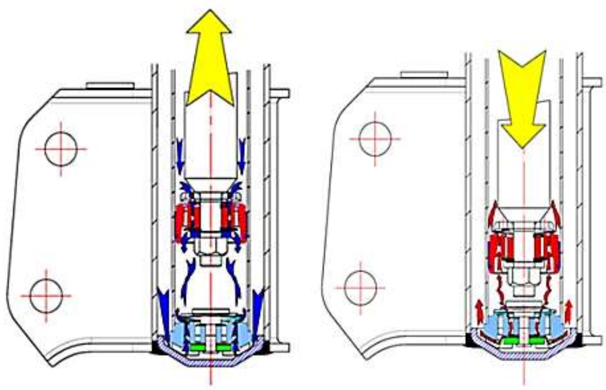

Fig. 3 : Fluid flow during operations

3 Experimental Tests

The hydraulic test rig is used to show how the damping force changes with the excitation velocity. The damper is fixed at one end on the test bench and is driven in translation attached to the other end, Figure 4. A load cell is installed on the fixed end of the damper. A data acquisition system records the damping force measurements and the corresponding displacements.

Three tests are carried out for different configurations of base and piston valves. For each test, the number and thicknesses of used metallic membranes are precise. Membranes play the role of valve spring in flow control. The number of valving orifices is fixed; 8 orifices for piston and 6 for base. The membrane configuration for each test is mentioned in Table 1 (Appendix), where e signifies the single membrane thickness.

The characteristics of test 1 are taken as initial values and conditions. For test 2, the modification concerned the piston valve, its stiffness is slightly reduced. For Test 3, the modification is made to the base valve, its stiffness is moderately reduced.

Fig. 4 : Test bench

The results of the calibration tests for three excitation velocities: 0.1, 0.3, and 0.5 m/s; and during the compression and rebound phases, are presented in the form of force-displacement curves, Figure 5, Figure 6 and Figure 7 in Appendix.

The upper part of the curves has positive velocities, corresponding to rebound, while the lower part of the curves has negative velocities, corresponding to compression. Either in rebound or in compression, the magnitude of damping force increases when the excitation velocity increases. The force increases and then decreases with displacement in nonlinear response for a given velocity. The measured values of the damping force in the three tests are shown in Table 2.

By modifying the configuration of the piston valve (Test 2), a slight variation is observed in the damping force of the two operating phases. The damping force increases by 2% in compression and rebound at the velocity of 0.1m/s. It increases by 1% in a rebound at the velocities 0.3 and 0.5 m/s, and it decreases by 4% and 3% in compression at the velocities 0.3 and 0.5m/s respectively.

By changing the base valve configuration (Test 3), a significant variation in the compression phase damping force is observed. The damping force increases by 13% in compression at a velocity 0.1m/s, and increases by 8% in compression at velocities 0.3 and 0.5 m/s. It decreases by 0.02%, 0.8% and 1.2% in rebound respectively at velocities 0.1 ,0.3, and 0.5m/s.

Table 2. Experimental values of damping force for three tests in compression and rebound

	Compression			Rubound		
Damping force (daN)	Piston velocity (m/s)			Piston velocity (m/s)		
	0,1	0,3	0,5	0,1	0,3	0,5
Test 1	51,3	93,4	117,5	28,4	50	71,3
Test 2	52,5	94,1	118,5	29	48	69,8
Test 3	58,4	101,1	127,7	28,1	49,6	70,5

The results of these three tests prove that the damping force increasing can be obtained in case of good choice of number and stiffness of membranes controlling piston and base valves outlets.

4 CFD Simulation

As a consequence of an experimental previous study, CFD simulation could be used to develop a numerical model helping in more understanding of the problem of valving. It also aims to enhance the design of the twin-tube hydraulic damper. The optimal solutions for design parameters can be found through an iterative process. The fluid velocities, pressure distribution, and resulting force on the rod of the damper depend strongly on the membranes stiffness and deformation. It’s a coupling fluid-structure problem.

4.1 Mathematical Background

When the piston acts, in compression or rebound direction, the fluid moves respectively through geometrical volume shown in Appendix in Figure 8 and Figure 9. Laminar and turbulent flows can happen. Fluid layers flow without mixing when the flow is laminar. When there is turbulence, the layers mix, and there are significant velocities in directions other than the axial direction of flow in the damper. Streamlines are smooth and continuous when the flow is laminar but break up and mix when the flow is turbulent. Turbulence main causes are obstruction or sharp corners and high speeds of fluid, [18], [19], and [20]. The excitation piston speed is generally low, so for the studied problem, the concentration should be more on laminar flow.

Poiseuille's law applies to the laminar flow of an incompressible fluid of viscosity η through a tube of length l and radius r. The direction of flow is from greater to lower pressure. Flow rate Q is directly proportional to the pressure difference ($P_2 - P_1$), and inversely proportional to the length l of the tube and viscosity η of the fluid, Eqs 1 to 3.
Flow is proportional to pressure difference and inversely proportional to resistance:

$$Q = \frac{P_2 - P_1}{R} \quad (1)$$

For laminar flow in a tube, Poiseuille's law for resistance states that:

$$R = \frac{8\eta l}{\pi r^4} \quad (2)$$

Poiseuille's law for flow in a tube is:

$$Q = \frac{(P_2 - P_1)\pi r^4}{8\eta l} \quad (3)$$

Poiseuille's law (Eq.3), shows that the flow rate Q through the damper valve holes depends stongly on the length l and radius r of holes. Therefore, the damping force applied on the rod of the damper is also influenced by the design parameters of the valves.

Ansys Fluent is used for CFD simulation. It provides comprehensive modeling capabilities for a wide range of incompressible and compressible, laminar, and turbulent fluid flow problems. Steady-state or transient analyses can be performed. A broad range of mathematical models is combined with the ability to model complex geometries. The mathematical model corresponding to laminar flow is chosen for the simulation of the studied hydraulic damper dynamics.

4.2 Simplified Geometrical Model and Meshing

Figure 8 (Appendix) presents the geometrical model filled by the fluid in the compression phase. The holes and the membrane zones of the base valve are considered. Based on that geometry a finite elements model is built using the software Ansys. The meshing is refined in confined zones.

The same work is done for the case of the rebound phase, Figure 9 (Appendix). The holes and membrane zones of the piston valve are considered in the model.

4.3 Dynamic Meshing

Hexahedral 3D-finite elements are more adequate for CFD problems. They generate for the model fewer elements and more nodes which provide more precision in results and make computation converge more rapidly than in the case of tetrahedral meshing. When the force is applied to the damper, the piston moves, and the fluid geometry changes in some zones. In stationary response, modification of meshing is not necessary. But in the case of transient response, a dynamic meshing should be considered. Three types of dynamic meshing can be applied in Ansys Fluent: Smoothing, layering, and remeshing. The two first methods are applicable to this problem, and they give similar results.

In the stationary case, the inlet velocity is applied to the piston face. But in transient response, the velocity of the subassembly piston-rod is applied at its mass center. This rigid body moves in the damper axis direction, its mass is $m_{rod\text{-}piston}$ = 1.15 kg for the experimental case study. At the outlet, the air or gas pressure is P_s = 1bar. The transient response duration is t_d = 0.1 s and the computation time step is Δt = 0.001 s.

4.4 Deflection of Membranes

In Appendix, Figure 10 presents the solution used for valve control. It consists of thin elastic membranes stuck with different thicknesses. For numerical simulation of membrane deformation, the points of application of pressure forces are situated on a circular contour passing through the centers of orifices outlets.
The determination of the membrane deflection on its boundary is conducted in steps described in Figure 11 (Appendix):

a) The CFD simulation starts with an initial value of deflection h=0.01 mm for a given velocity of the piston.
b) Evaluate force at the outlet of holes.
c) Apply the found force for a separate membrane structural model. For each hole corresponds a force.
d) The computation of that membrane structural model returns a new value of deflection
e) Restart the CFD simulation with the last value of deflection for the given velocity of the piston.

The method rule is to apply these steps till the deflection and hole outlet force remain constant. So, the method needs many iterations. For example, for the case of damper in compression for configuration C1 and for a piston velocity of 0.3 m/s the results of iterations are shown in Figure 12 (Appendix). The base valve membrane deflection is found h=0.34

mm. The same iterative method is also applied to determine the deflection of the piston membranes in the rebound phase for configuration D1. The piston valve membrane deflection is found h=0.28 mm.

4.5 Computation of Damping Force

Fluid in the damper is distributed in three chambers A, B, and C with average absolute pressures respectively P_1, P_2, and P_3. Damping forces in compression and rebound are determined by equilibrium equations respectively in Figure 13 and Figure 14. Friction forces and those due to atmospheric pressure on piston rod are neglected in comparison to main forces. *Ap* is the piston section side chamber B, and A_t is the piston-rod section. The extremity of the rod side piston is conical which induces a supplementary force F_{con} on the piston-rod. In the compression phase the damping force is given by equation (Eq.4) and in rebound it is given by equation (Eq.5).

$$F_{Compression} = P_2 A_p - P_1 (A_p - A_t) + F_{con} \tag{4}$$

$$F_{Rebound} = P_1 (A_p - A_t) - P_2 A_p + F_{con} \tag{5}$$

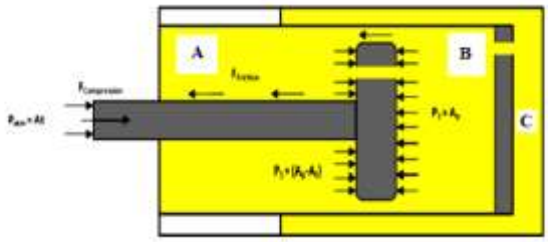

Fig. 13: Piston equilibrium-compression phase

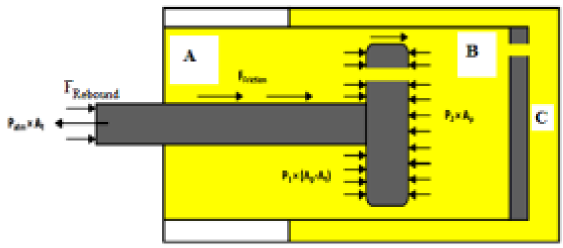

Fig. 14: Piston equilibrium-rebound phase

4.6 Numerical Results

For each numerical solution, the convergence is tested by verification of the residual curves. Velocity and continuity residuals should stay constant after enough iterations. As shown in Figure 15 the residuals' values are less than 0.001 and remain constants after 50 iterations, which confirms the convergence and acceptance of numerical solutions given by the software.

Numerical results presented in Appendix in Figure 16, Figure 17, Figure 18 and Figure 19, are all computed for piston velocity v=0.3 m/s. Figure 16 (Appendix) presents the disribution in compression in the case of configuration C1. Pressure can reach 7.32 bar in the compression chamber. Figure 17 (Appendix) shows the fluid flow velocity distribution in compression in the case of configuration C1. The high velocity of 12.95 m/s is found through the base valve orifices.

Figure 18 (Appendix) presents the distribution in a rebound in the case of configuration D1. Pressure can reach 8.44 bar in the rebound chamber. Figure 19 (Appendix) shows the fluid flow velocity distribution in a rebound in the case of configuration D1. The high velocity of 18.09 m/s is found through the piston valve orifices.

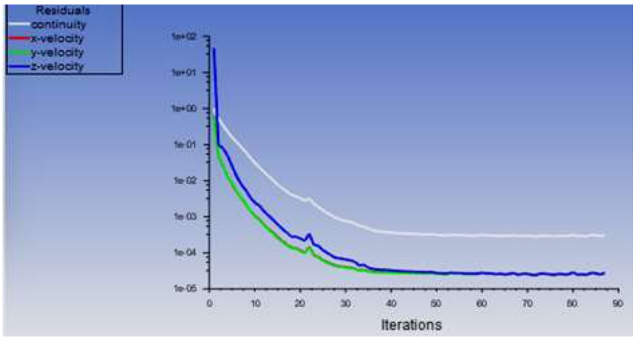

Fig. 15: Residuals curves to test convergence of numerical solution in case of configuration C1 and for v=0.3 m/s

5 Results comparison and Discussion

Figure 20 (Appendix) presents both numerical and experimental results on the same graph. The damping force is plotted function of the velocity of the damper piston. Curves are shown for both phases compression and rebound. For each phase are plotted two limit curves Dmax and Dmin for rebound and Cmax and Cmin for compression. They determine the acceptance zone for the tested damper. Results are plotted for configurations D1 and C1. The maximum damping force is obtained in the rebound phase. The results of the CFD simulation agree well with the measured data. That validates the numerical model of the twin-tube hydraulic damper.

The CFD model will be now applied to simulate more valve configurations. The choice of membrane stack for the base and piston is precised in Table 3 (Appendix). Numerical results are computed for piston velocity v=0.1 m/s. For both cases compression and rebound the upper limit, the lower limit, and the target value of damping force are defined and determined by the standards respecting to which vehicle the damper will be mounted, Table 3 (Appendix).

Figure 21 (Appendix) shows the damping force results in compression for different base valve membranes stack. For cases BMS2 and BMS4, values are out of limits. Cases BMS3 and BMS5 give acceptable values of damping force but are very close to limits. The stack BMS1 gives the nearest force to the target. It can be considered the best choice for the design of the damper base.

Figure 22 (Appendix) shows the damping force results in rebound for different piston valve membrane stacks. For cases, PMS2 to PMS5, force values exceed the upper limit. The stack PMS1 gives the nearest force to the target. It's the best choice for a damper piston.

The previous results show that the application of the numerical model, through an iterative computation of the membranes stack deflection, can give precisely the value of the damping force for a given piston velocity.

For different membrane stack configurations, without experimental testing, and without numerical simulations it is difficult to predict which one will give the nearest value to the target value of damping force. Considering the cost criterion, the numerical tool is the best and most rapid way to select the optimal valve configuration.

6 Conclusion

Testing a prototype of a hydraulic twin-tube dumper was useful to verify its performance in compression and rebound, under several excitation velocities, and with different configurations of the piston and base valves. The increasing of damping capacity or damping force is dependent on different parameters. The shim or membranes stack in pistons or base valves play the role of mechanical spring that controls fluid flow. The stiffness of such spring is an influencing parameter on the damper behavior. A numerical model was built and validated experimentally. The model was then applied to check the damping force value for different cases of shim stack of base and piston valves. The presented numerical model for a given twin-tube damper type can be applied for other automotive damper types by following the same calculation procedure and preparing the appropriate geometrical model. The presented method can contribute to the design of performant automotive dampers in terms of damping force.

Acknowledgement:
The authors thank the company « Leading Technology in Mechanics-LTM, Z.I Agba-Denden, Tunis, Tunisia » for the provision of experimental facilities.

References:

[1] Lang, H. H. (1977). *A Study of the Characteristics of Automotive Hydraulic Dampers at High Stroking Frequencies*. University of Michigan.

[2] Basso, R. (1998). Experimental characterization of damping force in shock absorbers with constant velocity excitation. *Vehicle System Dynamics*, 30(6), 431-442. https://doi.org/10.1080/00423119808969459

[3] Chahine, R. (2011). *Modeling of a World Rally Championship Car Damper and Experimental Testing of Its Components*. The Royal Institute of Technology, Department of Aeronautical and Vehicle Engineering, Vehicle Dynamics Division, Stockholm. Master's Thesis, pp. 1-59. https://kth.diva-portal.org/smash/get/diva2:503320/FULLTEXT01.pdf (Last Accessed Date : 18/12/24)

[4] Solomon, U., & Padmanabhan, C. (2011). Hydro-gas suspension system for a tracked vehicle: Modeling and analysis. *Journal of Terramechanics*, 48(2), 125-137. https://doi.org/10.1016/j.jterra.2010.12.001

[5] Tare, H. K., & Patil, S. R. (2016). Experimental Characterization of Gas Filled Hydraulic Damper Using Ramp Excitation. *International Journal of Scientific Research in Science, Engineering and Technology*2 (5), 504-513. https://ijsrset.com/home/issue/view/article.php?id=IJSRSET16261 (Last Accessed Date : 18/12/24)

[6] Koch, G., Pellegrini, E., Spirk, S., & Lohmann, B. (2010). *Design and modeling of a quarter-vehicle test rig for active suspension control*. Technische Universitat Munchen. Technical Reports on Automatic Control Vol. TRAC-5, pp. 1-28. https://mediatum.ub.tum.de/doc/1072356/document.pdf (Last Accessed Date 13/12/24)

[7] Hou, Y., Li, L., He, P., Zhang, Y., Chen, L., & Center, C. (2011, March). Shock absorber modeling and simulation based on modelica. *In Proceedings of the 8th International Modelica Conference* (No. 063, pp. 843-846). Dresden, Germany.

[8] Gällsjö, A., & Johansson, M. (2012). *Physical Modelling and Automatic Configuration of CES Valve*. Linköping University, The Institute of Technology, Sweden. Master's

thesis, pp. 1-72. https://liu.diva-portal.org/smash/get/diva2:539767/FULLTEXT01.pdf (Last Accessed Date : 13/12/24)

[9] Gao, B., Darling, J., Tilley, D. G., Williams, R. A., Bean, A., & Donahue, J. (2005). Non-linear modelling of a novel gas strut. *Proceedings of the Institution of Mechanical Engineers, Part D: Journal of Automobile Engineering*, 219(10), 1153-1164. https://doi.org/10.1243/095440705X34874

[10] Ferdek, U., & Łuczko, J. (2012). Modeling and analysis of a twin-tube hydraulic shock absorber. *Journal of Theoretical and Applied Mechanics*, 50(2), 627-638. http://www.ptmts.org.pl/jtam/index.php/jtam/article/view/v50n2p627 (Last Accessed Date : 15/12/24)

[11] Henrik Skagerstrand, (2014). *Shock absorber modelling*. Division of Vehicle Engineering and Autonomous Systems, Chalmers University of Technology, Göteborg, Sweden. Master's Thesis, pp. 1-90. https://publications.lib.chalmers.se/records/fulltext/211571/211571.pdf (Last Accessed Date : 10/12/24)

[12] Konieczny, Ł. (2016). Analysis of simplifications applied in vibration damping modelling for a passive car shock absorber. *Shock and Vibration*, Volume 2016, 9 pages. https://doi.org/10.1155/2016/6182847

[13] Bhuyan, D., & Kumar, K. (2016). Design and analysis of base valve of twin tube dampers. *Applied Mechanics and Materials*, 852, 504-510. https://doi.org/10.4028/www.scientific.net%2FAMM.852.504

[14] Jugulkar, L. M., Singh, S., & Sawant, S. M. (2016). Fluid flow modeling and experimental investigation on automobile damper. *Construction and Building Materials*, 121, 760-772. https://doi.org/10.1016/j.conbuildmat.2016.05.142

[15] Guan, D., Jing, X., Shen, H., Jing, L., & Gong, J. (2019). Test and simulation the failure characteristics of twin tube shock absorber. *Mechanical Systems and Signal Processing*, 122, 707-719. https://doi.org/10.1016/j.ymssp.2018.12.052

[16] Farjoud, A., Ahmadian, M., Craft, M., & Burke, W. (2012). Nonlinear modeling and experimental characterization of hydraulic dampers: effects of shim stack and orifice parameters on damper performance. *Nonlinear Dynamics*, 67, 1437-1456. https://doi.org/10.1007/s11071-011-0079-2

[17] Yu, L., Wei, W., Yanlei, L., Wei, D., & Limei, Z. (2022). Orifice Frequency Dispersion Characteristics Effect on Hydraulic System Pressure Pulsation. *Iranian Journal of Science and Technology, Transactions of Mechanical Engineering*, 46, 793-803. https://doi.org/10.1007/s40997-022-00487-z

[18] Richardson, S. M. (2011). *Poiseuille Flow*. In Thermopedia. Begel House Inc. https://doi.org/10.1615/AtoZ.p.poiseuille_flow

[19] Constantinescu, V. N. (2012). *Laminar viscous flow*. Mechanical Engineering Series. Springer New York, NY. Edition 1, 488 pages. https://doi.org/10.1007/978-1-4612-4244-4

[20] Cengel, Y., & Cimbala, J. (2019). *Fluid mechanics: fundamentals and applications, 4e in SI Units*. McGraw-Hill Education,. 1021 pages. https://books.google.tn/books/about/Fluid_Mechanics_Fundamentals_and_Applica.html?id=KcKlDwAAQBAJ&redir_esc=y (Last Accessed Date : 12/12/24)

Contribution of Individual Authors to the Creation of a Scientific Article (Ghostwriting Policy)

The authors equally contributed to the present research, at all stages from the presentation of the problem, experimental testing, to the numerical solution and final findings.

Sources of Funding for Research Presented in a Scientific Article or Scientific Article Itself

No funding was received for conducting this study.

Conflict of Interest

The authors have no conflicts of interest to declare.

APPENDIX

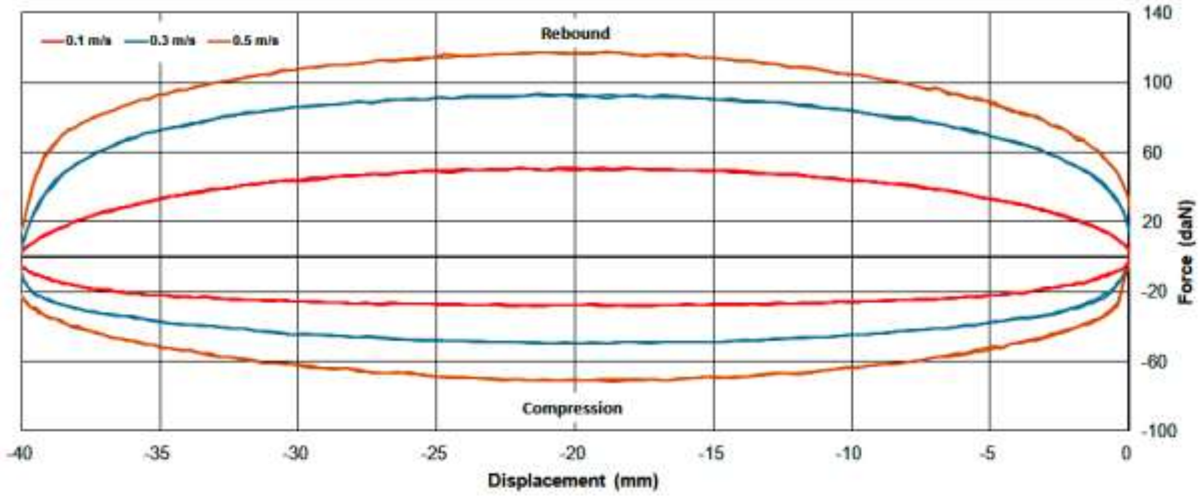

Fig. 5: Result of test 1, Force-displacement curves

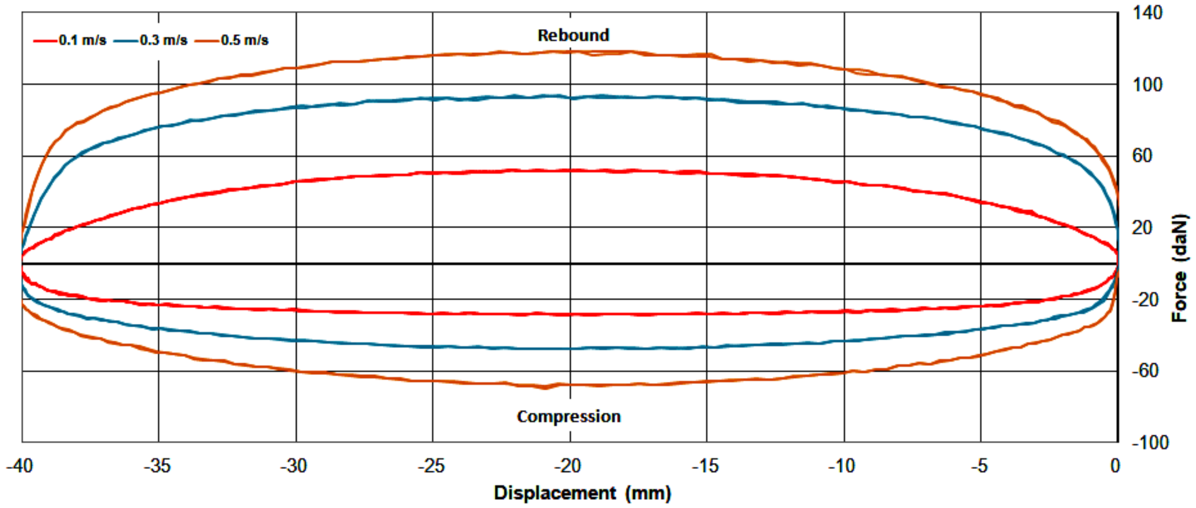

Fig. 6 : Result of test 2, Force-displacement curves

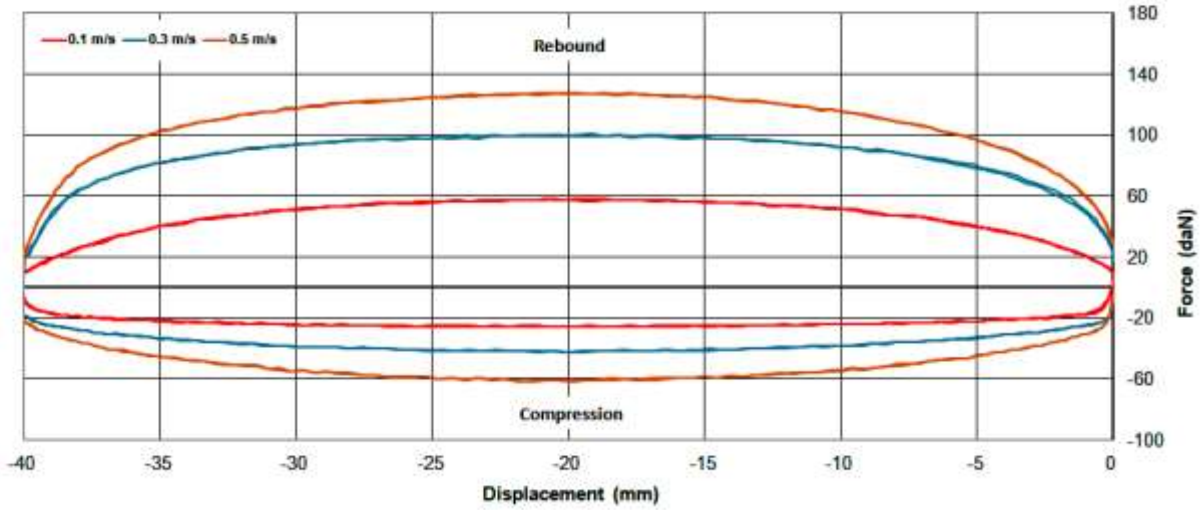

Fig. 7 : Result of test 3, Force-displacement curves

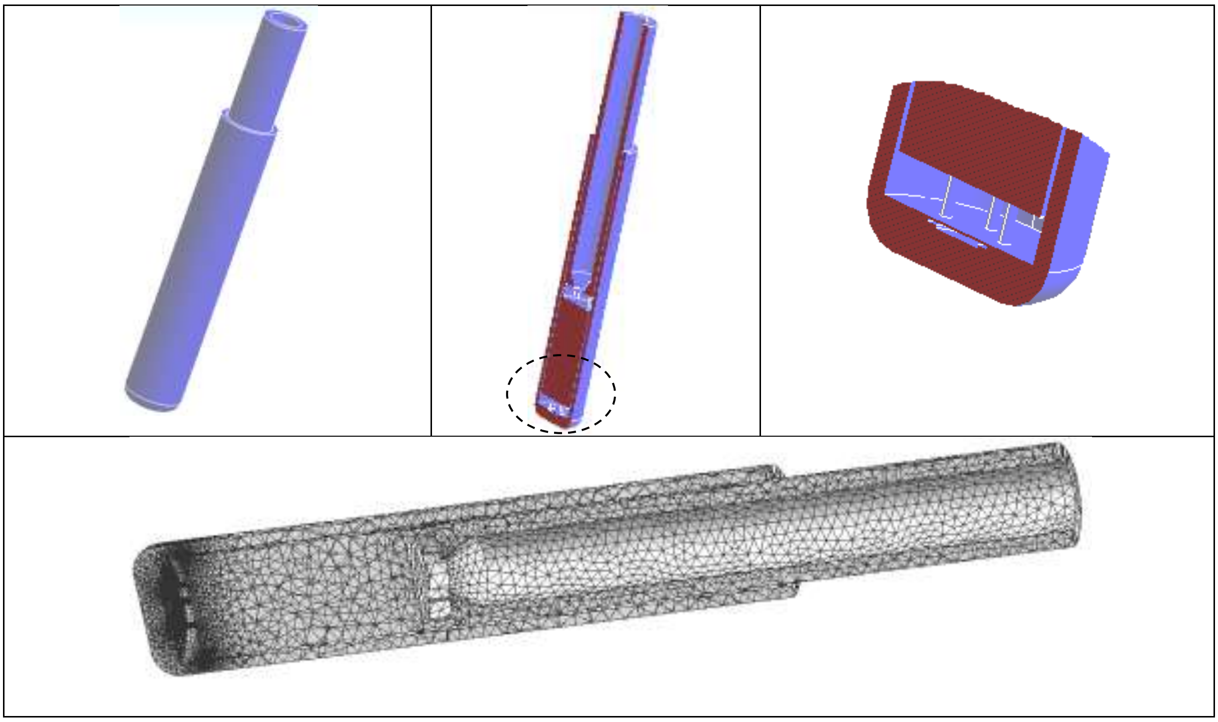

Fig. 8 : Geometrical model and meshing for compression phase

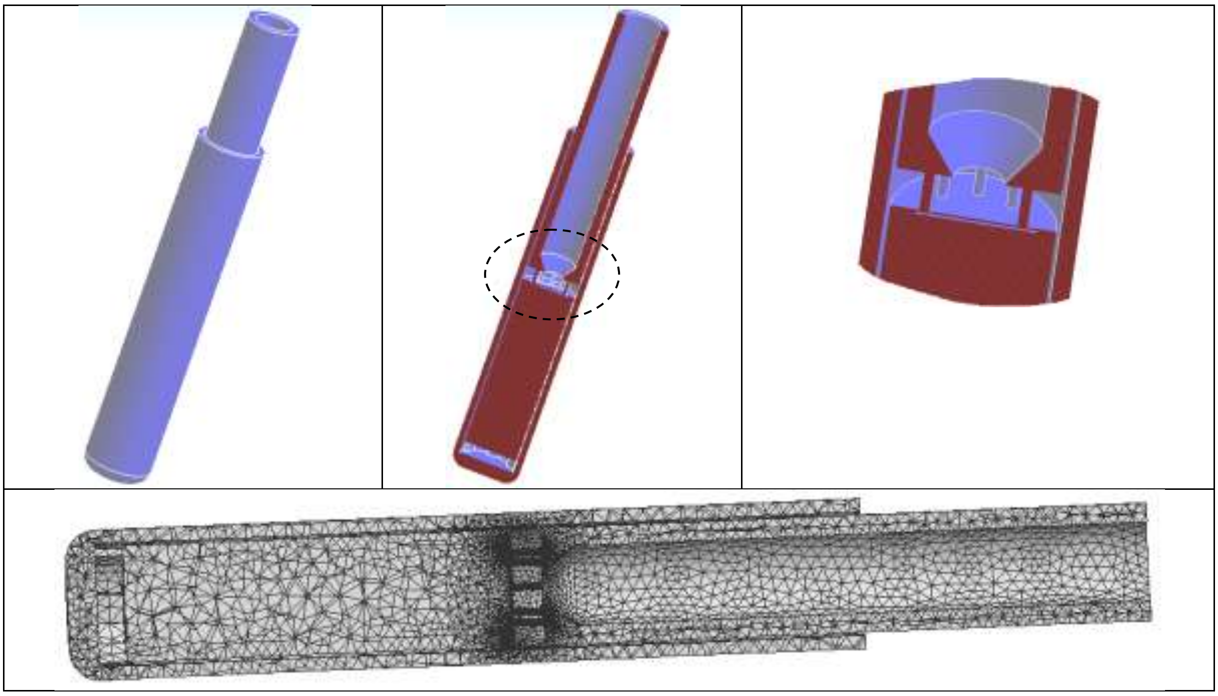

Fig. 9 : Geometrical model and meshing for rebound phase

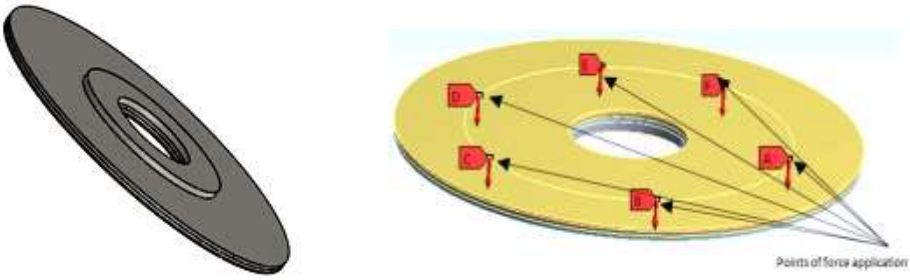

Fig. 10: Design of membranes for valve control and points of application of forces due to pressure of outlet flow through orifices

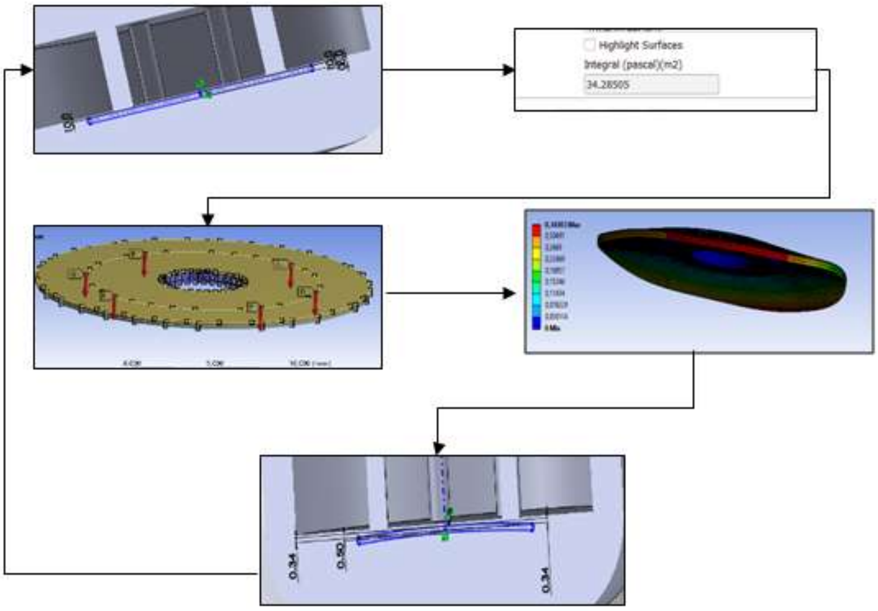

Fig. 11: Iterative method for computation of membrane deflection for given piston velocity

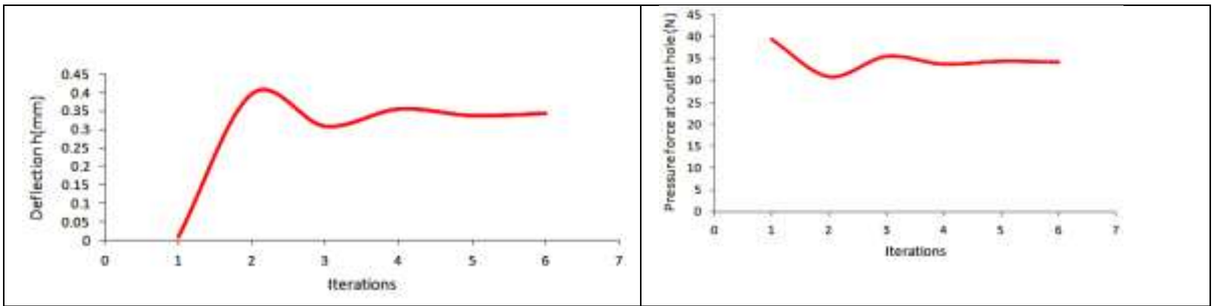

(a)	(b)

Fig. 12: Results of iterative method : (a) membrane deflection (b) force at hole outlet

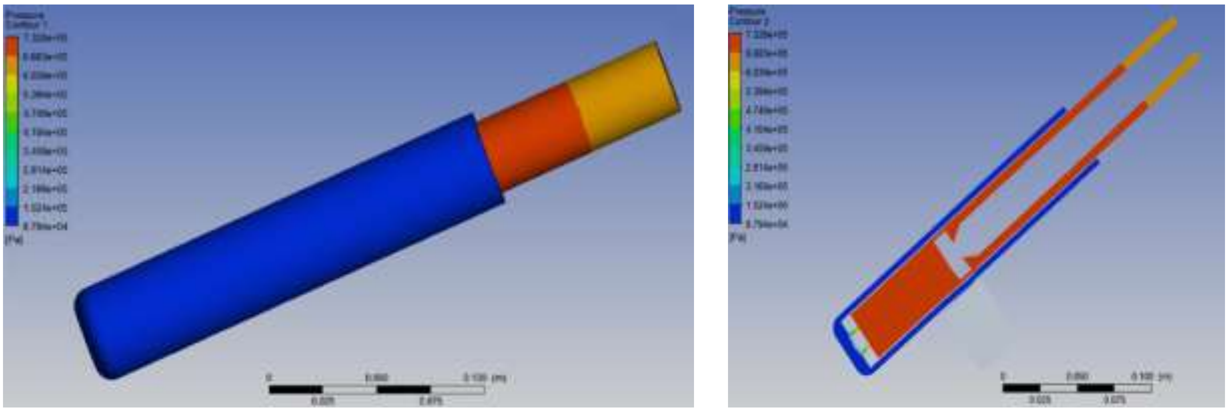

(a) (b)

Fig. 16: Pressure distribution in compression in case of configuration C1 and for v=0.3 m/s : (a) outside view (b) section view through two base valve holes

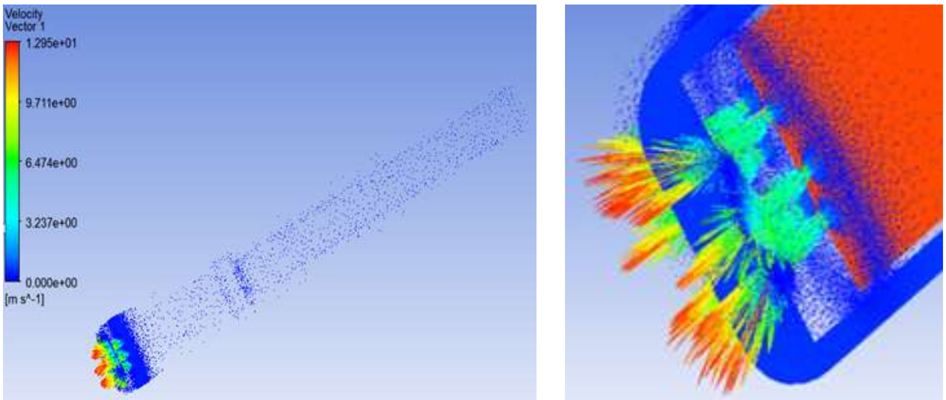

(a) (b)

Fig. 17 : Fluid flow velocity distribution in compression in case of configuration C1 and for v=0.3 m/s : (a) 3D view (b) flow through base valve holes

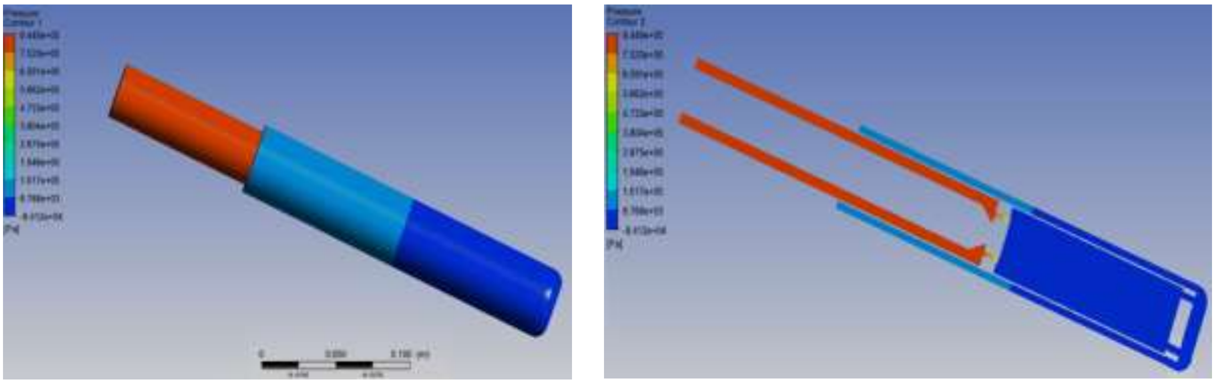

(a) (b)

Fig. 18 : Pressure distribution in rebound in case of configuration D1 and for v=0.3 m/s : (a) outside view (b) section view through two piston valve holes

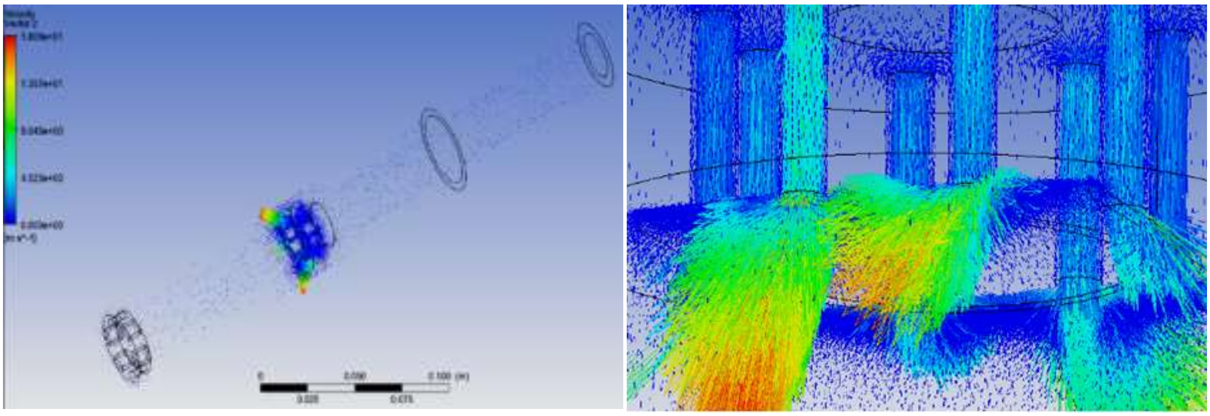

(a) (b)

Fig. 19 : Fluid flow velocity distribution in rebound in case of configuration D1 and for v=0.3 m/s : (a) 3D view (b) flow through piston valve holes

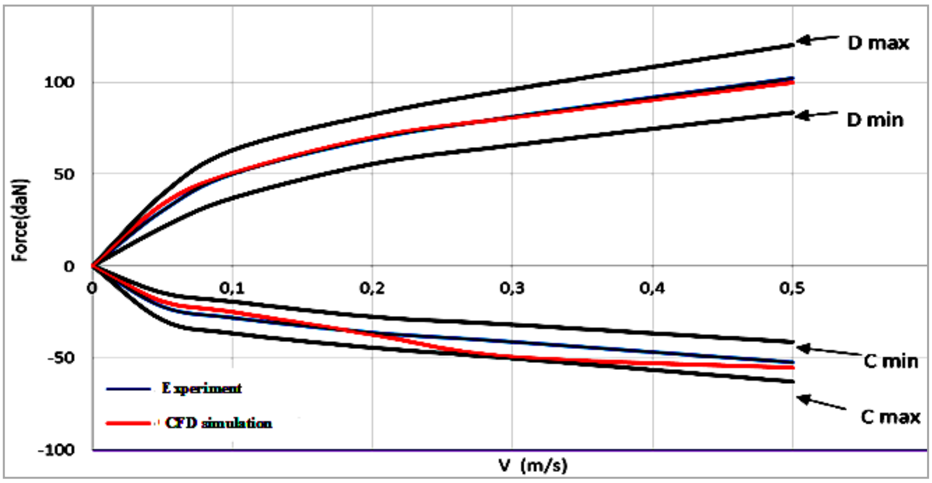

Fig. 20: CFD simulation and experimental results comparison

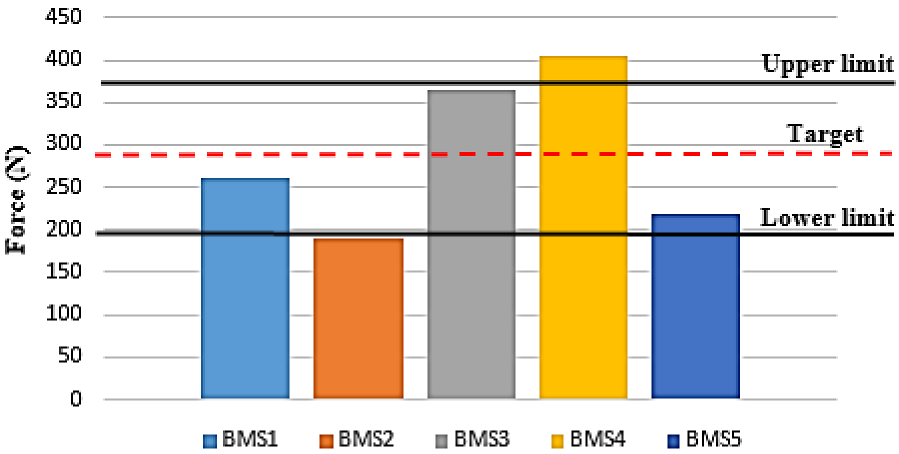

Fig. 21: Model results- Damping force for different stacks of base membranes

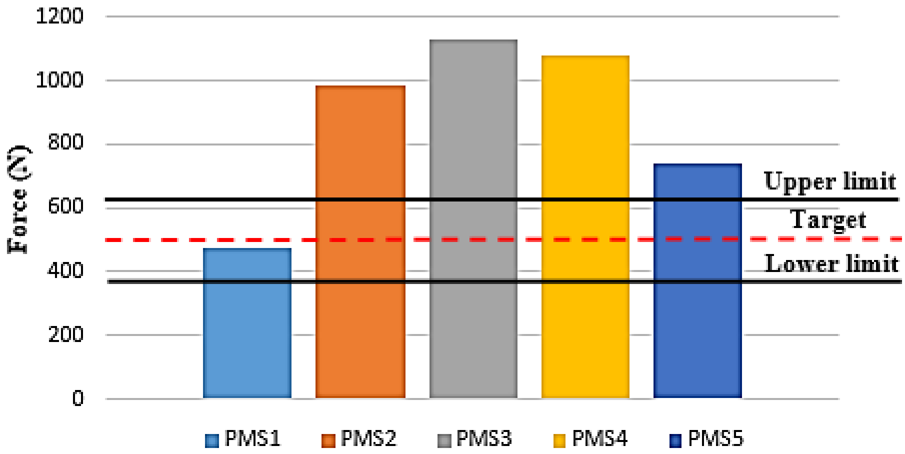

Fig. 22: Model results- Damping force for different stacks of piston membranes

Table 1. Configuration of membranes in three tests

	Base valve	Piston valve
Test 1	**C1:** 5 membranes with e=0.1 mm	**D1:** 1 membrane with e=0.1 mm and 2 notch flow 3 membranes with e=0.1 mm 1 membrane with e=0.2 mm
Test 2	**C2:** 5 membranes with e=0.1 mm	**D2:** 1 membrane with e=0.1 mm and 2 notch flow 2 membranes with e=0.2 mm
Test 3	**C3:** 1 membrane with e=0.1 mm 1 membrane with e=0.2 mm	**D3:** 1 membrane with e=0.1 mm and 2 notch flow 3 membranes with e=0.1 mm 1 membrane with e=0.2 mm

Table 3. Configurations of valve membranes stack

Base membranes stack (BMS) – Compression Upper limit=366 N ; Lower limit=192 N Target=280 N		Piston membranes stack (PMS) – Rebound Upper limit=630 N ; Lower limit=370 N Target=500 N	
BMS1	5 membranes with e=0.1 mm	**PMS1**	5 membranes with e=0.1 mm
BMS2	1 membranes with e=0.1 mm 2 membranes with e=0.2 mm	**PMS2**	1 membranes with e=0.1 mm 2 membranes with e=0.2 mm
BMS3	2 membranes with e=0.1 mm 1 membranes with e=0.3 mm	**PMS3**	2 membranes with e=0.1 mm 1 membranes with e=0.3 mm
BMS4	1 membranes with e=0.2 mm 1 membranes with e=0.3 mm	**PMS4**	1 membranes with e=0.2 mm 1 membranes with e=0.3 mm
BMS5	3 membranes with e=0.1 mm 1 membranes with e=0.2 mm	**PMS5**	3 membranes with e=0.1 mm 1 membranes with e=0.2 mm